Earthquakes and Structures, *Vol. 11, No. 1 (2016) 165-178*
DOI: http://dx.doi.org/10.12989/eas.2016.11.1.165

Estimation of earthquake induced story hysteretic energy of multi-Story buildings

Feng Wang*[1], Ning Zhang[2a] and Zhiyu Huang[1b]

[1]*College of Civil Engineering, Dalian Minzu University, Dalian, China*
[2]*Dalian Polytechnic University, Dalian, China*

(Received January 28, 2016, Revised June 22, 2016, Accepted June 28, 2016)

Abstract. The goal of energy-based seismic design is to obtain a structural design with a higher energy dissipation capacity than the energy dissipation demands incurred under earthquake motions. Accurate estimation of the story hysteretic energy demand of a multi-story structure is the key to meeting this goal. Based on the assumption of a mode-equivalent single-degree-of-freedom system, the energy equilibrium relationship of a multi-story structure under seismic action is transformed into that of a multi-mode analysis of several single degree-of-freedom systems. A simplified equation for the estimation of the story seismic hysteretic energy demand was then derived according to the story shear force and deformation of multi-story buildings, and the deformation and energy relationships between the mode-equivalent single-degree-of-freedom system and the original structure. Sites were categorized into three types based on soil hardness, namely, hard soil, intermediate hard (soft) soil, and soft soil. For each site type, a 5-story and 10-story reinforced concrete frame structure were designed and employed as calculation examples. Fifty-six earthquake acceleration records were used as horizontal excitations to validate the accuracy of the proposed method. The results verify the following. (1) The distribution of seismic hysteretic energy along the stories demonstrate a degree of regularity. (2) For the low rise buildings, use of only the first mode shape provides reasonably accurate results, whereas, for the medium or high rise buildings, several mode shapes should be included and superposed to achieve high precision. (3) The estimated hysteretic energy distribution of bottom stories tends to be underestimated, which should be modified in actual applications.

Keywords: hysteretic energy demand; nonlinear response history analysis; pushover analysis; equivalent SDOF system; earthquake excitation

1. Introduction

With the advances of performance-based earthquake engineering, the displacement-based design has been adequately promoted, whereby inelastic analysis is necessary for determining the displacement demands. However, previous seismic damage and theoretical analyses have identified not only insufficient deformation ability, but also insufficient energy dissipation

*Corresponding author, Associate Professor, E-mail: win_0803@163.com
[a]Associate Professor, E-mail: zhangninglady@sina.com
[b]Ph.D. Student, E-mail: zyhuang1978@163.com

 ISSN: 2092-7614 (Print), 2092-7622 (Online)

capacity as essential factors of the structure damage and collapse incurred during strong earthquakes. Cumulative energy is an important index to estimate damaging potential of earthquake excitations and earthquake resistant capacities of structures that is the basis of the energy-based seismic design (EBSD).

In an EBSD method, the inelastic energy is utilized as a main design parameter in which the accumulation of earthquake induced damage can be taken into account in the design procedure. In the 1950s, Housner proposed the use of energy analysis methods to analyze structural seismic response. In the 1980s, Akiyama employed the results of energy analyses to define the fundamental concepts involved with EBSD methods, which have since been included in Japan's seismic standards. In the 1990s, Fajfar first adopted the Park-Ang model to transform structural cumulated hysteretic energy into the elevation of structural ductility demand, and the displacement ductility index was used to assess structural damage. Thereafter, EBSD was further explored, and various seismic design methods were established. For example, Bruneau (1996) proposed a standardized EBSD program to estimate the nonlinear response of single-degree-of-freedom (SDOF) systems. Decanini and Mollaioli (2001) proposed an EBSD program for the estimation of structural seismic energy demand. Meanwhile, Estes and Anderson (2002) investigated the distribution of hysteretic energy along a structure's stories, and presented some beneficial conclusions. Leelataviwat and Gol (2002) proposed an EBSD program based on the structural yield mechanism and target displacement. Choi and Kim (2006) proposed an EBSD procedure for designing framed structures with buckling-restrained braces in which the hysteretic energy spectra and accumulated ductility spectra were used. Ghosh and Collins (2006) explored a concept in which an EBSD criterion and the reliability-based methods were merged. Arroyo and Ordaz (2007) proposed a rule to estimate hysteretic energy demands that depended on the elastic pseudo acceleration and velocity spectra. Prasanth, Ghosh, and Collins (2008) employed modal pushover analysis to estimate structural hysteretic energy. Benavent-Climent (2011) proposed an EBSD seismic assessment program to evaluate the seismic performance of existing frame structures. Habibi, Chan, and Albermani (2013) proposed an EBSD procedure for retrofitting structures with passive energy dissipation systems. Wang and Li (2015) proposed a procedure for estimating hysteretic energy of multistory structures based on the normalized hysteretic energy spectrum.

Peak energy, corresponding to the strongest earthquake in the region, should be calculated to evaluate seismic performance of structures when applying the EBSD procedure to design structures. If various peak energy values are plotted as a function of a natural period, the resulting energy spectrum could then be used to determine the energy demand of a particular system to a specific type of excitation. Trends in the various energy spectra have been developed for several areas of research, such as earthquake input energy spectrum (Amiri *et al*. 2008, Benavent-Climent *et al*. 2010, Wang and Li 2015), hysteretic energy spectrum (Riddell and Garcia 2001, Wang and Li 2015), absorbed energy spectrum (Chou and Uang 2000), momentary energy spectrum (Hagiwara 2000), and inelastic cyclic demand spectrum (Kunnanth and Chai 2004). For the several kinds of energy spectra, the absorbed energy spectrum is essentially the equivalent velocity spectra of maximum absorbed energy which is used to reflect the demand of absorbed energy (or hysteretic energy); the momentary energy spectrum is essentially the equivalent velocity spectrum of momentary input energy; the inelastic cyclic demand spectrum is the relation between the inelastic cyclic numbers and vibration period which can be used to analyze the cumulative damage.

The goal of EBSD is to obtain a structural design with a higher energy dissipation capability than the energy dissipation demand incurred during earthquakes. A common process of EBSD is,

first, to estimate the total energy demand of the structure via the energy spectrum under the equivalent SDOF system assumption, and then to determine the seismic energy demand of each story according to the regularity of energy distribution along structural stories. In this method, the implementation of EBSD relies on determining the relationship between the energy dissipation of the equivalent SDOF system and that of the original structure subjected to earthquake motions. Moreover, the regularity of energy distribution along structural stories must also be determined. Due to the complexity of the structural parameters and the uncertainty of ground motion, a degree of randomness is inherent in the research objective, which is the key challenge encountered in current EBSD studies, and is therefore investigated in the present study.

2. Principle

2.1 Energy balance equation of modal SDOF systems

Consider an n-story plane-symmetric building. The equation of motion governing the responses of the n-story building subjected to earthquake excitation $\ddot{u}_g(t)$ along the direction of the horizontal principal axis is given as follows

$$\mathbf{M}\ddot{\mathbf{u}}(t)+\mathbf{C}\dot{\mathbf{u}}(t)+\mathbf{F}(t)=-\mathbf{M}\boldsymbol{\iota}\ddot{u}_g(t) \tag{1}$$

where $\mathbf{M}$ is the diagonal mass matrix, $\mathbf{C}$ is the damping matrix, $\mathbf{u}(t)$ is the displacement response vector, given as $[u_1(t)\ u_2(t)\ \ldots\ u_n(t)]$, $\mathbf{F}(t)$ is the resisting forces vector, and the vector $\boldsymbol{\iota}$ represents the $1\times n$ identity matrix [1 1 … 1]. According to Eq. (1), the energy balance equation of the considered building can be derived as

$$\int_0^{t_0} d\mathbf{u}(t)^T\mathbf{M}\ddot{\mathbf{u}}(t)+\int_0^{t_0} d\mathbf{u}(t)^T\mathbf{C}\dot{\mathbf{u}}(t)+\int_0^{t_0} d\mathbf{u}(t)^T\mathbf{F}(t)=-\int_0^{t_0} d\mathbf{u}(t)^T\mathbf{M}\boldsymbol{\iota}\ddot{u}_g(t) \tag{2a}$$

Here, t_0 is the duration of earthquake motion, and $\dot{\mathbf{u}}(t)dt$ is equal to $d\mathbf{u}(t)$, where $\dot{\mathbf{u}}(t)$ is the velocity vector. Eq. (2a) can be simplified as

$$E_k(t)+E_d(t)+E_h(t)=E_I(t) \tag{2b}$$

where $E_k(t)$, $E_d(t)$, $E_h(t)$, and $E_I(t)$ are the kinetic energy, viscous damping energy, hysteretic energy, and input energy, respectively, of the considered building. In a static procedure, such as pushover analysis, a major hypothesis is that the responses of buildings can be expressed as a superposition of the responses of appropriate SDOF systems just like in the linear range (Kalkan and Kunnath 2007). As such, $\mathbf{u}(t)$ for an inelastic system can be expanded in terms of the natural vibration modes of the corresponding linear elastic system

$$\mathbf{u}(t)=\sum_{i=1}^{n}\mathbf{u}_i(t)=\sum_{i=1}^{n}\boldsymbol{\varphi}_i x_i(t) \tag{3}$$

where $\boldsymbol{\varphi}_i$ is the i-th mode shape vector, given as $[\phi_{i,1},\ \phi_{i,2},\ldots,\ \phi_{i,n}]$, and $\mathbf{u}_i(t)$ is the linear displacement response vector of the i-th modal, given as $[u_{i,1}(t),\ u_{i,2}(t),\ \ldots,\ u_{i,n}(t)]$. Eq. (3) is substituted into Eq. (2a), and, after pre-multiplying both sides of the adjusted equation by $\boldsymbol{\varphi}_i^T$, the following equations can be derived.

$$\int_0^{t_0} \boldsymbol{\varphi}_i^T \mathbf{M} \boldsymbol{\varphi}_i \ddot{x}_i(t)\dot{x}_i(t)dt + \int_0^{t_0} \boldsymbol{\varphi}_i^T \mathbf{C} \boldsymbol{\varphi}_i \dot{x}_i(t)\dot{x}_i(t)dt + \int_0^{t_0} F_i(t)\dot{x}_i(t)dt = -\int_0^{t_0} \boldsymbol{\varphi}_i^T \mathbf{M} \boldsymbol{\varphi}_i \gamma_i \ddot{u}_g(t)\dot{x}_i(t)dt \ (i=1,...n) \quad (4a)$$

in which the i-th modal resisting force $F_i(t)$ can be represented as $\boldsymbol{\varphi}_i^T \mathbf{K}_p(t) \boldsymbol{\varphi}_i x_i(t)$, where $\mathbf{K}_p(t)$ is the elastic-plastic instantaneous stiffness matrices. Eq. (4a) can be simplified as

$$E_{k,i}(t) + E_{d,i}(t) + E_{h,i}(t) = E_{I,i}(t) \qquad (i = 1, \mathrm{L}\ , n) \quad (4b)$$

where $E_{k,i}(t)$, $E_{d,i}(t)$, $E_{h,i}(t)$, and $E_{I,i}(t)$ are the kinetic energy, viscous damping energy, hysteretic energy, and input energy, respectively, of the i-th modal of the considered building. In Eq. (4a), the modal participation factor γ_i can be expressed as

$$\gamma_i = \frac{\boldsymbol{\varphi}_i^T \mathbf{M} \boldsymbol{\iota}}{\boldsymbol{\varphi}_i^T \mathbf{M} \boldsymbol{\varphi}_i} \quad (5)$$

In Eq. (4a), $\boldsymbol{\varphi}_i^T \mathbf{M} \boldsymbol{\varphi}_i$ can be represented by $m_{eq,i}$, which is interpreted as the i-th modal equivalent mass. Both sides of Eq. (4a) are divided by $\gamma_i^2 m_{eq,i}$, and, employing the orthogonality of modes, the uncoupled equations can be derived as

$$\int_0^{t_0} \ddot{q}_i(t)\dot{q}_i(t)dt + \int_0^{t_0} 2\xi\omega_i \dot{q}_i(t)\dot{q}_i(t)dt + \int_0^{t_0} F_{eq,i}(t)\dot{q}_i(t)dt = -\int_0^{t_0} \ddot{u}_g(t)\dot{q}_i(t)dt \quad (i = 1,...,n) \quad (6a)$$

where ω_i is the i-th natural vibration frequency, ξ is the damping ratio, the displacement response $q_i(t)$ is equal to $x_i(t)/\gamma_i$, and the resisting force $F_{eq,i}(t)$ is equal to $F_i(t)/\gamma_i m_{eq,i}$. Eq. (6a) can be simplified as

$$e_{k,i}(t) + e_{d,i}(t) + e_{h,i}(t) = e_{I,i}(t) \qquad (i = 1, \cdots, n) \quad (6b)$$

where $e_{k,i}(t)$, $e_{d,i}(t)$, $e_{h,i}(t)$, and $e_{I,i}(t)$ are the kinetic energy, viscous damping energy, hysteretic energy, and earthquake input energy of the i-th modal equivalent SDOF system, respectively.

Dissipated hysteretic energy is the structural response parameter which is often correlated to cumulative damage (Fajfar and Vidic 1994). So, this research should aim at developing expressions to compute hysteretic energy demands. Comparing $e_{h,i}$, $E_{h,i}$, and E_h, the following relationship is obtained

$$E_h(t) = \sum_{i=1}^{n} E_{h,i}(t) = \sum_{i=1}^{n} m_{eq,i} \cdot \gamma_i^2 \cdot e_{h,i}(t) \quad (7)$$

2.2 Demand of story hysteretic energy

According to Eq. (4), the hysteretic energy of the j-th story of the i-th mode can be expressed as

$$E_{h,i}^j(t_0) = \int_0^{t_0} V_{i,j}(t)\dot{v}_{i,j}(t)dt \qquad (i = 1, \cdots, n) \quad (8)$$

where $V_{i,j}(t)$ and $v_{i,j}(t)$ are the momentary shear force and drift of the j-th story of the i-th mode, respectively, and $v_{i,j}(t)=u_{i,j}(t)-u_{i,j-1}(t)$. According to the previous derivation, $u_{i,j}(t)$ is approximately equal to $\phi_{i,j}\gamma_i q(t)$ where $\phi_{i,j}$ is the mode shape value of the j-th story of the i-th mode shape $\boldsymbol{\varphi}_i$. In

addition, $V_{i,j}(t)$ and $v_{i,j}(t)$ may be expanded as follows

$$V_{i,j}(t) \approx \sum_{l=j}^{n} F_{i,l}(t) \approx \sum_{l=j}^{n} m_l \phi_{i,l} A_i(t) \gamma_i \; ; \quad v_{i,j}(t) \approx \Delta\phi_{i,j} q_i(t) \gamma_i \tag{9}$$

Here, $F_{i,l}(t)$ is the resisting force of the l-th story of the i-th mode, m_l is the mass of the l-th story, $A_i(t)$ is the pseudo acceleration response of the i-th modal equivalent SDOF system, and $\Delta\phi_{i,j} = \phi_{i,j} - \phi_{i,j-1}$. Substituting Eq. (9) into Eq. (8), and according to Eq. (7), the hysteretic energy of the j-th story can be rewritten as

$$E_h^j(t_0) \approx \sum_{i=1}^{m} \int_0^{t_0} V_{i,j}(t) \dot{v}_{i,j}(t) dt \approx \sum_{i=1}^{m} \int_0^{t_0} (\sum_{l=j}^{n} m_l \phi_{i,l}) \Delta\phi_{i,j} \gamma_i^2 A_i(t) \dot{q}_i(t) dt \tag{10}$$

where $E_h^j(t_0)$ is the hysteretic energy of the j-th story of the considered building. According to the definition of pseudo acceleration (Fajfar 1999) and Eq. (6a), the following relationship is obtained

$$\int_0^{t_0} A_i(t) \dot{q}_i dt \approx e_{h,i}(t_0) \tag{11}$$

Substituting an earthquake motion duration t_1 for t_0, the equation for estimating story hysteretic energy is expressed as

$$E_h^j(t_1) \approx \sum_{i=1}^{n} \left((\sum_{l=j}^{n} m_l \phi_{i,l}) \Delta\phi_{i,j} \gamma_i^2 e_{h,i}(t_1) \right) \qquad (j = 1, \cdots, n) \tag{12}$$

Herer $\phi_{i,l}$ is the mode shape value of the l-th story of the i-th mode shape $\boldsymbol{\varphi}_i$. For a low rise building, the lateral deformation is mainly influenced by the first mode shape $\boldsymbol{\varphi}_1$, and the effects of higher modes can be ignored. So the equation for estimating story hysteretic energy can be rewritten as

$$E_h^j(t_1) \approx (\sum_{l=j}^{n} m_l \phi_{1,l}) \Delta\phi_{1,j} \gamma_1^2 e_{h,1}(t_1) \qquad (j = 1, \cdots, n) \tag{13}$$

Considering variation of mode shape in plastic response range of buildings, the mode shapes in Eqs. (12) and (13) can be replaced by $\boldsymbol{\varphi}_{p,i}$ ($\boldsymbol{\varphi}_{p,i}$=[$\phi_{p,i,1}$, $\phi_{p,i,2}$,……, $\phi_{p,i,n}$]) and $\boldsymbol{\varphi}_{p,1}$ ($\boldsymbol{\varphi}_{p,1}$=[$\phi_{p,1,1}$, $\phi_{p,1,2}$,……, $\phi_{p,1,n}$]), respectively, which can be gotten by pushover analysis or modal pushover analysis (Poursha *et al*. 2011, Camara and Astiz 2012, Manoukas *et al*. 2012, Wang and Zhang 2014). The Eq. (12) or Eq. (13) can be regarded as the simplified method to estimate structural story hysteretic energy.

3. Numerical example

3.1 Description of the example building model

In order to clarify how the proposed method should be applied, for hard soil site, intermediate hard (soft) soil site and soft soil site, six simple analytical examples are presented. For each soil

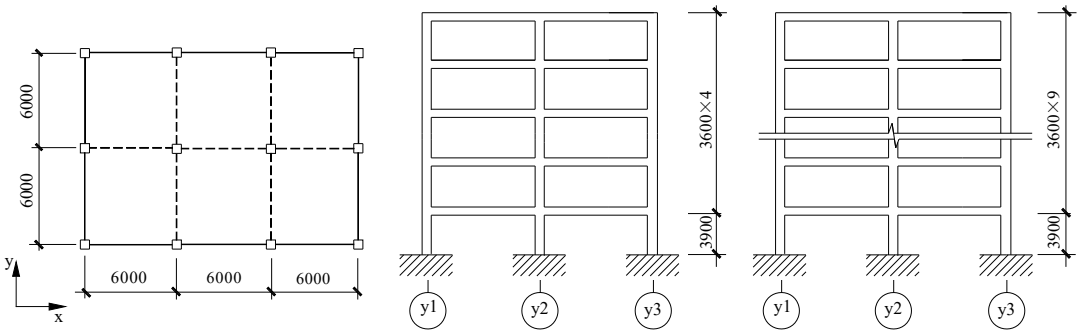

(a) Ichnography (b) Section plans of the 5-story and 10-story building models

Fig. 1 Sketch of the example building models (unit: mm)

site, the structures considered are a 5-storey and a 10-storey symmetric reinforced concrete frame buildings, illustrated in Fig. 1. It is considered that the ground motion is acting along y axis. Each floor diaphragm is rigid in its own plane. The dimension in height and plane are shown as the Fig. 1. For the six buildings: the sectional sizes of beams are 300 mm×500 mm for all the buildings; the sectional sizes of columns are 500 mm×500 mm for all the buildings. Concrete compression strength is designed as 20 MPa for all beams, and 30 MPa for all columns. The design dead load and live load of each floor (roof) are 6.5 kN/m^2 (4.7 kN/m^2), 1.0 kN/m^2 (2.0 kN/m^2) respectively. for each floor (roof). The damping of the example building is modeled by the Rayleigh damping, and damping ratio ξ equals 5%. The horizontal shear strengths of the buildings for different soil sites are different. Steel ratios are approximately 1.5% for beam sections and 2% for column sections.

The example building is simplified as a nonlinear multi-story frame model. The criteria reflecting conditions of strong columns and weak beams, strong shear and weak bending, and strong joints and weak components are used for designing the example building. As such, the restoring force relations of the beam-column joints are assumed to be the linear elastic model, and the restoring force relations for the bending of two beam (and column) ends are assumed to be the bilinear stiffness degradation model, where the yield stiffness coefficient is 0.03 and the stiffness degradation coefficient is 0.4. The story mass matrices **M** are given with corresponding diagonal terms 400 t, 450 t, 450 t, 450 t, 450 t, 450 t, 450 t, 450 t, 450 t, 500 t for the 10-story building model, and 400 t, 450 t, 450 t, 450 t, 500 t for the 5-story building model.

3.2 Earthquake acceleration records

For verifying the accuracy of the proposed simplified method, the results of the simplified method are compared with the results of the nonlinear response history analysis (NL-RHA) method, in which the acceleration records of earthquake motions are used. 56 earthquake acceleration records for hard soil site (Vs=360-750 m/s), intermediate hard (soft) soil site (Vs=180-360 m/s) and soft soil site (Vs<180 m/s), corresponding to B, C and D respectively for USGS, are selected and listed in Table 1. The rules for selecting these records are defined as: (1) Magnitude=6~8; (2) Fault distance=15 km~45 km; (3) Peak acceleration≥0.1 g, approximately. The peak ground accelerations (PGA) of the records are adjusted to 3.0 m/s^2 and 5.1 m/s^2, respectively.

Table 1 Information obtained from earthquake acceleration records for three soil types

Sites	No.	Stations	Earthquakes	Components	No.	Stations	Earthquakes	Components
Hard soil site	1	1095 Taft Lincolnhool	Kern County (52/7/21,Ms7.7)	TAF021	11	57504 Coyote Lake Dam	Loma Prieta (89/10/18,Ms7.1)	CLD195
	2			TAF111	12			CLD285
	3	1652 Anderson Dam(Downstrea)	Loma Prieta (89/10/18,Ms7.1)	AND270	13	TCU047	Chi-Chi, Taiwan (99/9/20,Ms7.6)	TCU047-N
	4			AND360	14			TCU047-W
	5	24157LA-Baldwin Hills	Northridge (94/1/17,Ms6.7)	BLD090	15	57383 Gilroy Array #6	Loma Prieta (89/10/18,Ms7.1)	G06000
	6			BLD360	16			G06090
	7	14403 LA-116th St School	Northridge (94/1/17,Ms6.7)	116090	17	58378 APEEL 7-Pulgas	Loma Prieta (89/10/18,Ms7.1)	A07000
	8			116360	18			A07090
	9	23 Coolwater	Landers (92/6/28,Ms7.4)	CLW-LN	19	24611 LA-Temple & Hope	Northridge (94/01/17,Ms6.7)	TEM090
	10			CLW-TR	20			TEM180
Intermediate hard (soft) soil site	21	90016 LA-N Faring Rd	Northridge (94/1/17,Ms6.7)	FAR000	31	Iznik	Kocaeli (99/08/17,Ms7.8)	IZN180
	22			FAR090	32			IZN090
	23	6621 Chihuahua	Imperial Valley (79/10/15,Ms6.9)	CHI012	33	135LA-Hollywood Stor Lot	San Fernando (71/02/09,Ms6.6)	PEL090
	24			CHI282	34			PEL180
	25	22074 Yermo Fire Station	Landers (92/6/28,Ms7.4)	YER270	35	6621 Chihuahua	Victoria (80/06/09,Ms6.4)	CHI102
	26			YER360	36			CHI192
	27	Bolu	Duzce (99/11/12,Ms7.3)	BOL000	37	47125 Capitola	Morgan Hill (84/04/24,Ms6.1)	CAP042
	28			BOL090	38			CAP132
	29	36227 Parkfield Cholame 5W	Coalinga (83/05/02,Ms6.5)	H-C05270	39	90091 LA-Saturn St	Northridge (94/1/17,Ms6.7)	STN020
	30			H-C05360	40			STN110
Soft soil site	41	5057 El Centro Array #3	Imperial Valley (79/10/15,Ms6.9)	H-E03140	49	0 Kakogawa	Kobe (95/01/16,Ms6.9)	KAK000
	42			H-E03230	50			KAK000
	43	9001 Montebeel-BR	Northridge (94/1/17,Ms6.7)	BLF206	51	Ambarli	Kocaeli (99/08/17,Ms7.8)	ATS000
	44			BLF296	52			ATS090
	45	CHY104	Chi-Chi (99/9/20,Ms7.6)	CHY104-E	53	1002 APEEL 2-Redwood City	Loma Prieta (89/10/18,Ms7.1)	A02043
	46			CHY104-N	54			A02133
	47	0 Shin-Osaka	Kobe (95/01/16,Ms6.9)	SHI000	55	58117 Treasure Island	Loma Prieta (89/10/18,Ms7.1)	TRI000
	48			SHI090	56			TRI090

3.3 Distribution characteristics of hysteretic energy

The peak ground acceleration (PGA) of the earthquake acceleration records listed in Table 1 were adjusted to 3.0 m/s^2 and 5.1 m/s^2, respectively, and were input along y axis direction of the considered building models. Nonlinear response history analysis (NL-RHA) was performed to obtain the hysteretic energy value $E_{h,i}$ for each story i. If various $E_{h,i}$ are plotted as a function of story i, the resulting curves could then be used to determine the hysteretic energy distribution along stories of the buildings under a single earthquake excitation record. However, significant differences in the values of $E_{h,i}$ may be obtained under different earthquake excitation records, and the hysteretic energy distribution obtained under each earthquake excitation should be normalized to obtain statistically meaningful hysteretic energy distribution patterns. Specifically, the normalized story hysteretic energy α_i is defined as the ratio of $E_{h,i}$ to the total hysteretic energy summed over all stories i, such that $\sum\alpha_i$=1.

Figs. 2 and 3 present distributions of α for the 5-story building model subjected to earthquake excitations with PGA of 3.0 m/s^2 and 5.1 m/s^2, respectively, which correspond to the moderate earthquake and the strong earthquake with the fortification intensity of 8. In each figure, the fine lines are the distribution curves of α for different earthquake excitations, and the solid line is the statistically averaged distribution curve of α, expressed as μ, and the two dashed lines are the distribution curves for 'μ+1.645×σ' and 'μ-1.645×σ', respectively, in which μ is the average value of α, and σ is the standard deviation of α. It can be seen that the distributions of α exhibit a degree of regularity for different soil types and peak seismic accelerations, where α decreases with increasing i, with a maximum α obtained at the bottom story (i=1) in accordance with an inverse triangular distribution. This is similar to a lateral structural deformation pattern. This may be because the first mode of the bottom structure controls the lateral structural deformation and horizontal seismic force distribution. Because the hysteretic energy is the result of integrating the product of the horizontal deformation and seismic force, α exhibits an approximately inverse triangular distribution.

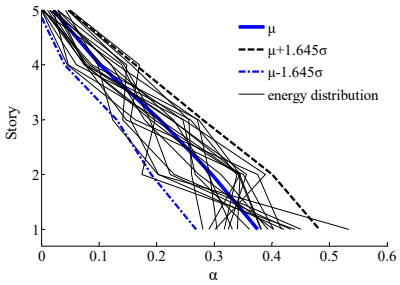

(a) Hard soil site

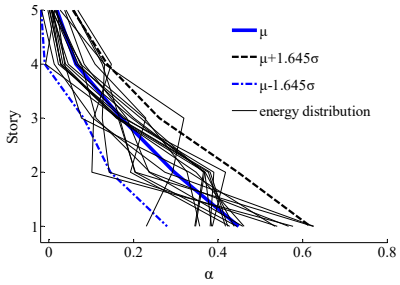

(b) Intermediate hard (soft) soil site

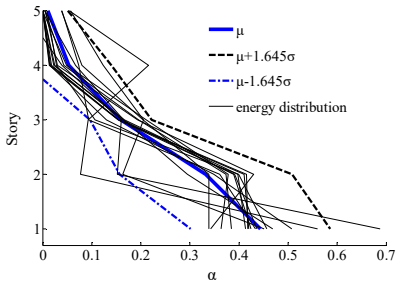

(c) Soft soil site

Fig. 2 The hysteretic energy distribution of the 5-story model (PGA=3.0 m/s^2)

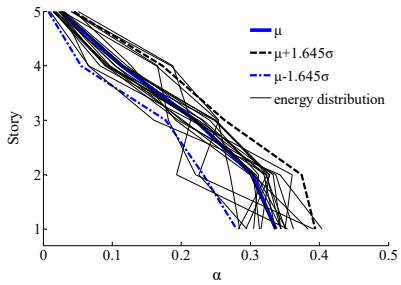

(a) Hard soil site

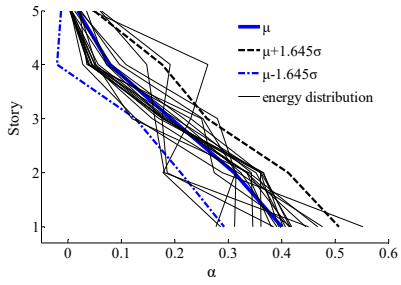

(b) Intermediate hard (soft) soil site

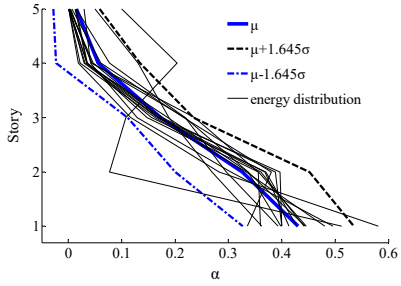

(c) Soft soil site

Fig. 3 The hysteretic energy distribution of the 5-story model (PGA=5.1 m/s^2)

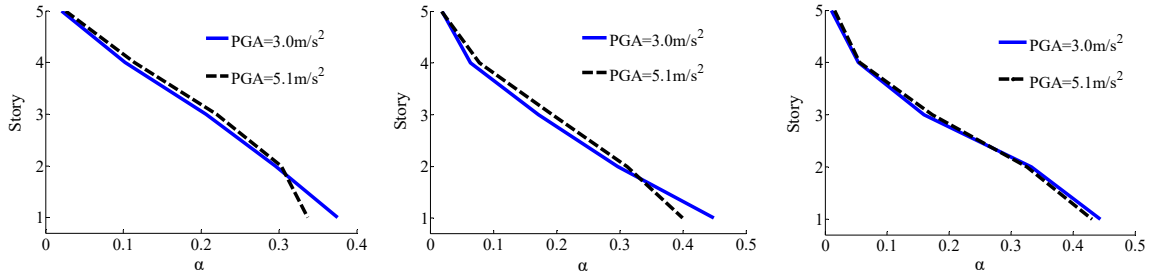

(a) Hard soil site (b) Intermediate soil site (c) Soft soil site

Fig. 4 Comparison of the average hysteretic energy distributions for the 5-story building model under earthquake excitations with PGA of 3.0 m/s^2 and 5.1 m/s^2

Fig. 4 shows a comparison of the average values of α obtained for the 5-story building model under earthquake excitation with PGA of 3.0 m/s^2 and 5.1 m/s^2. It can be observed that α exhibits consistent distributions along stories for different soil sites, and that the bottom story under earthquake excitation with PGA of 3.0 m/s^2 has a small average α, particularly in hard and intermediate hard (soft) soil sites. Meanwhile, the comparison of the dashed lines in Figs. 2 and 3 indicates that the dispersion in the values of α for the PGA of 5.1 m/s^2 is reduced relative to that for the PGA of 3.0 m/s^2. This may be because the development of story plasticity is influenced by the PGA. Specifically, the high PGA will result in the sufficient plastic response for each story of the building. For the PGA of 3.0 m/s^2, the structural plastic developmental states of the stories vary under different earthquake excitations, where, for some earthquake excitations, the stories even remain in the elastic response range, showing substantial dispersion. For the PGA of 5.1 m/s^2, the structural stories are in the plastic response range, and exhibit similar plastic development for different stories, so the degree of dispersion is small.

Figs. 5 and 6 present distributions of α for the 10-story building model under earthquake excitation with PGA of 3.0 m/s^2 and 5.1 m/s^2, respectively. As given in Figs. 2 and 3, the fine lines are the distribution curves of α for each earthquake wave excitation, and the solid line is the statistically averaged distribution curve of α, and the two dashed lines are the distribution curves for 'μ+1.645×σ' and 'μ-1.645×σ', respectively. Compared with the 5-story building model, the distributions of α for the 10-story building model do not conform to an inverse triangular pattern, but decrease smoothly from the bottom story with increasing i, and no energy concentrations are observed at the bottom, middle, and top stories, indicating that the influence of high modes on the lateral deformation pattern of the medium or high rise buildings is not negligible.

Comparison of the dispersion of the distributions of α for different soil types indicates that the level of dispersion decreases in the order of soft soil, intermediate hard (soft) soil, and, finally, hard soil. This is because strong earthquake excitation can result in the concentration of hysteretic energy in some stories, which dramatically alters the energy distribution pattern, and the concentration of hysteretic energy will become increasingly apparent with increasing plastic deformation. Moreover, the characteristics of structural hysteretic energy concentration vary under different earthquake excitation. As such, with increasingly soft extent of soil, the extent of plastic deformation of the structures increases, which results in the increase of extent of hysteretic energy concentration, and the increase of differences in the energy distribution characteristics under different earthquake wave excitations. Thus, the dispersion of α distributions of soft soil site is the largest in the three soil types, and in contrast, that of hard soil site is the least. For the 10-story

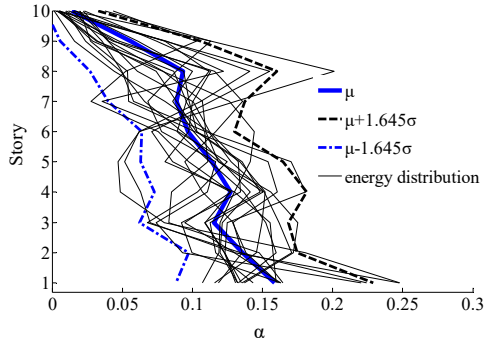

(a) Hard soil site

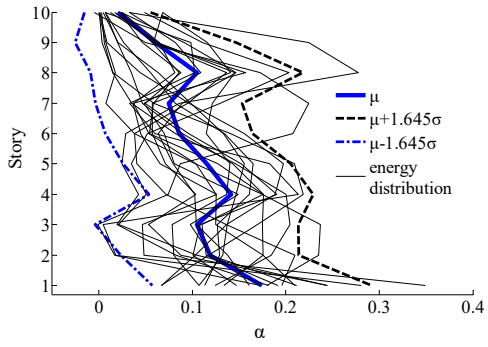

(b) Intermediate hard (soft) soil site

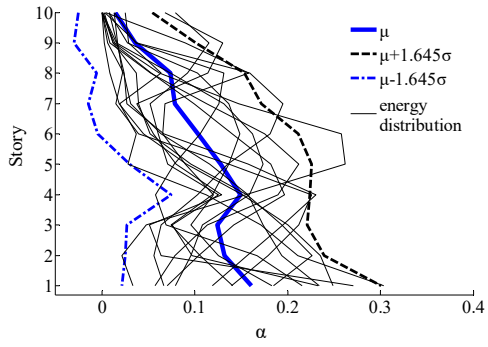

(c) Soft soil site

Fig. 5 The hysteretic energy distribution of the 10-story model (PGA=3.0 m/s^2)

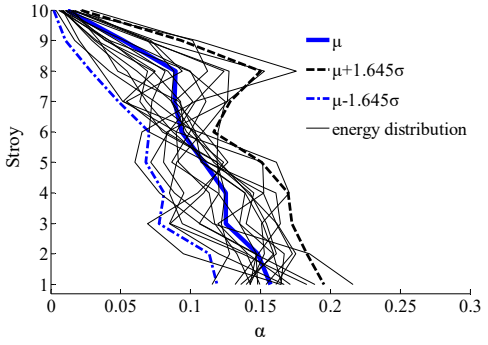

(a) Hard soil site

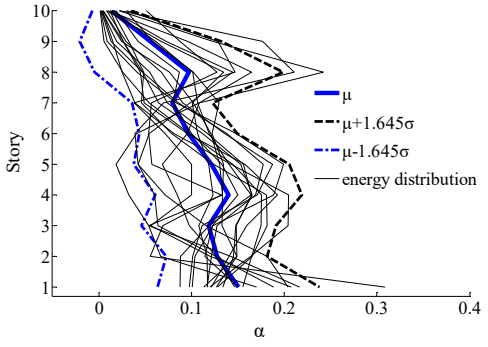

(b) Intermediate hard (soft) soil site

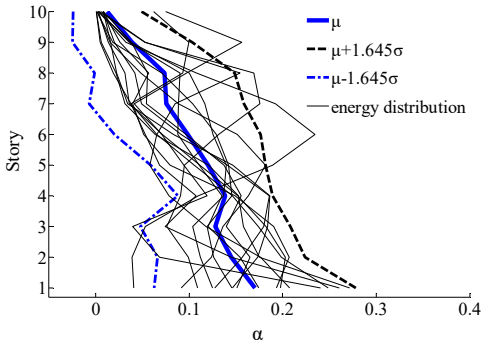

(c) Soft soil site

Fig. 6 The hysteretic energy distribution of the 10-story model (PGA=5.1 m/s^2)

building model, as was found with the 5-story building model, the degree of dispersion of the distribution of α under the earthquake excitations of 5.1 m/s^2 is smaller than that under the excitations of 3.0 m/s^2.

Fig. 7 shows a comparison of the average values of α for the 10-story building model under the earthquake excitations with PGA of 3.0 m/s^2 and 5.1 m/s^2. It can be seen that the distributions of the average α at the two accelerations are similar, which suggests that, differencing from the 5-story building model, the 10-story building model subjected to earthquake excitations with PGA of 3.0 m/s^2 demonstrates a degree of plastic deformation for each structural story.

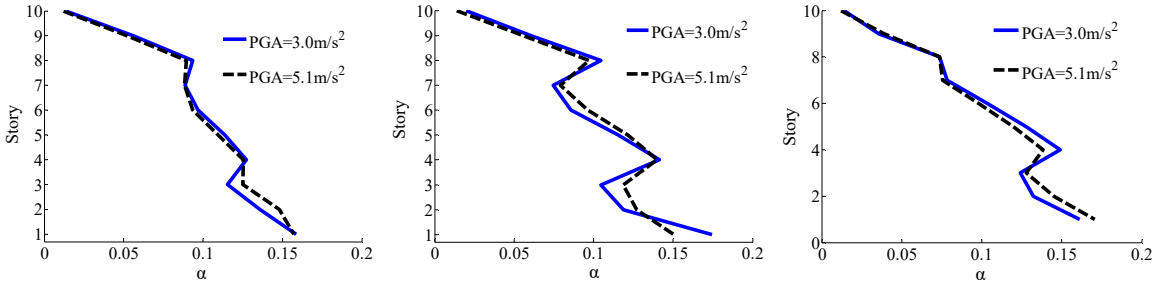

(a) Hard soil site (b) Intermediate soil site (c) Soft soil site

Fig. 7 Comparison of the average hysteretic energy distributions for the 10-story building model under earthquake excitations with PGA of 3.0 m/s^2 and 5.1 m/s^2

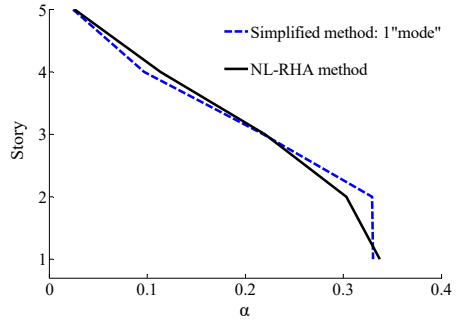

(a) Hard soil site

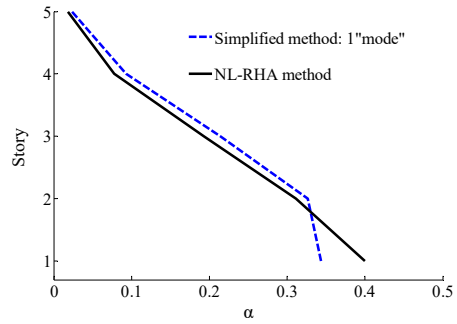

(b) Intermediate hard (soft) soil site

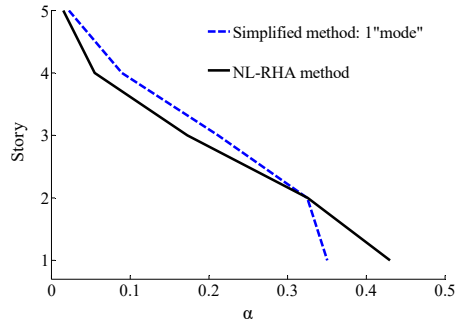

(c) Soft soil site

Fig. 8 Comparison of the results of the two methods for the 5-story model

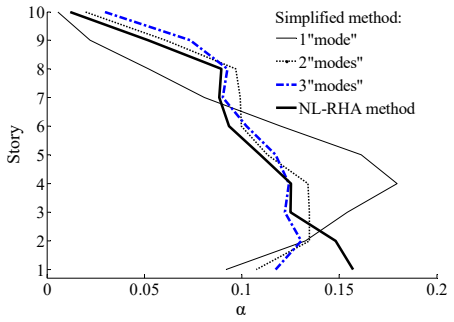

(a) Hard soil site

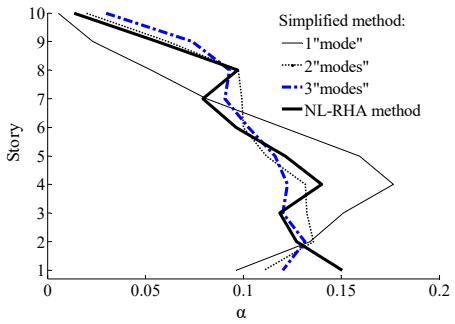

(b) Intermediate hard (soft) soil site

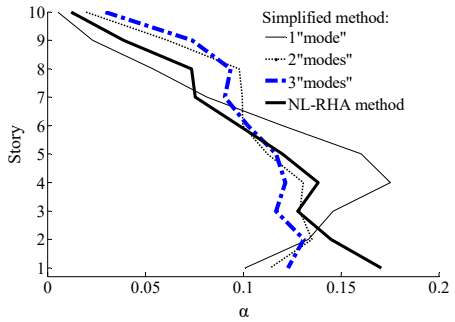

(c) Soft soil site

Fig. 9 Comparison of the results of the two methods for the 10-story model

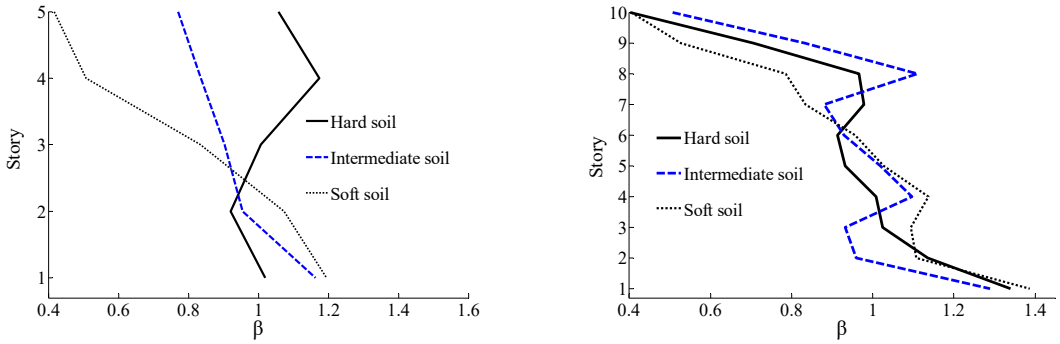

(a) 5-story building model (b) 10-story building model

Fig. 10 The bias of the simplified method

3.4 Comparison of results for the two methods

The story hysteretic energy calculation method (see Eqs. (12) and (13)) in this study is referred to as the simplified method. Assuming that the average results of the nonlinear response history analysis (NL-RHA) represent exact solutions, the accuracy of the simplified method can be validated by comparing the results of α distributions obtained by the simplified method with those obtained by the NL-RHA method. Previous analysis indicates that the hysteretic energy distribution under moderate earthquake exhibits substantial degree of dispersion, so that the hysteretic energy can be determined according to the conservatively applied assumption that every story resides in the plastic response range. With this assumption, the distributions of α under strong earthquake can be analyzed and compared. Figs. 8 and 9 present a comparison of the two methods in terms of the distribution curves of α obtained under the earthquake excitations with PGA of 5.1 m/s^2 for the 5-story and 10-story building models.

The following observations can be made. (1) Based on the assumption that the deformation pattern of a low rise building is mainly controlled by the first mode shape, so that only the first mode shape is included for estimating the distribution of α, the figure shows that the form of the distribution for the 5-story model is essentially accurate, except that the bottom story has an underestimated value of α, which must be corrected for an actual application. (2) The distribution of α for the 10-story building model was estimated in the simplified method by including only the first mode shape, the first and second mode shapes, or the first three lowest-order mode shapes. The results show that, when including only the first mode, the estimation results exhibit a large bias, but that the estimation results including the first 2 or 3 mode shapes demonstrate a good accuracy in tendency, with only small differences between them. As was observed for the 5-story building model, the bottom story again exhibits an underestimated value of α, which must also be corrected for actual applications.

3.5 Analysis of the bias of the simplified method

To analyze the estimation bias of the simplified method, β is defined as the ratio of the α-values obtained by the NL-RHA method to those obtained by the simplified method. A comparison between the values of β obtained for the three different types of soil and structures comprised of 5 and 10 stories is shown in Fig. 10. Because conditions where $\beta \leq 1$ are acceptable, only biases with

β>1, denoted as a positive bias, were considered. The following can be observed from Fig. 10. (1) The positive biases of the three different types of soil are small for the 5-story building model. However, the distribution of the bias varies according to the soil type. Specifically, the fourth story for the hard soil and the bottom story for the intermediate hard (soft) and soft soil sites have large biases that are close to 1.2, which are larger than those of the other stories. (2) For the 10-story building model, the bottom story has a positive bias as large as 1.4, whereas the other stories have smaller positive biases.

4. Conclusions

The estimation of earthquake induced hysteretic energy demand of each story of multi-story structures is one of the key challenges of the EBSD method. In this study, the story hysteretic energy demand was derived according to the energy equilibrium equation of a multi-story building subjected to earthquake excitations when employing the modal equivalent SDOF system assumption combined with the structure shear force and deformation relationship under earthquake excitations. In the proposed simplified method, the mode shapes in the plastic response range were substituted for the elastic mode shapes. The following conclusions from this study can be drawn.

• The distribution of hysteretic energy along a structure's stories exhibits a degree of regularity that is not influenced by the soil type, but is dramatically influenced by the total number of stories. For the low rise buildings, the distribution of α exhibits an inverse triangular form, which is similar to lateral structural deformation patterns. In contrast, the distribution of α for the medium or high rise buildings does not conform to the inverse triangular pattern owing to the influences of high-order mode shapes, but decreases smoothly from the bottom story to the top story, and, except for the bottom story, both middle and high stories exhibit energy concentrations.

• The simplified method can precisely estimate the distribution characteristics of earthquake induced hysteretic energy along a structure's stories. In conjunction with an appropriate modification for the bottom story, the story hysteretic energy demand can be accurately obtained.

Acknowledgements

This research described in this paper was financially supported by the National Natural Science Foundation of China (Grant No. 51478091), the Program for Liaoning Excellent Talents in University (Grant No. LJQ2014139), and the project of Dalian Nationalities University (Grant No. DC201502040301).

References

Amiri, G.G., Darzi, G.A. and Amiri, J.V. (2008), "Design elastic input energy spectra based on Iranian earthquakes", *Can. J. Civ. E.*, **35**(6), 635-646.

Arroyo, D. and Ordaz, M. (2007), "On the estimation of hysteretic energy demands for SDOF systems", *Earth. Eng. Struct. Dyn.*, **36**(15), 2365-2382.

Benavent-Climent, A. (2011), "A energy-based method for seismic retrofit of existing frames using hysteretic dampers", *Soil. Dyn. Earthq. Eng.*, **31**(10), 1385-1396.

Benavent-Climent, A., Lopez-Almanse, F. and Bravo-Gonzalez, D.A. (2010), "Design energy input spectra

for moderate-to-high seismicity regions based on Colombian earthquakes", *Soil. Dyn. Earthq. Eng.*, **30**(11), 1129-1148.
Bruneau, M. and Wang, N. (1996), "Normalized energy-based methods to predict the seismic ductile response of SDOF structures", *Eng. Struct.*, **18**(1), 13-28.
Camara, A. and Astiz, M.A. (2012), "Pushover analysis for the seismic response prediction of cable-stayed bridges under multi-directional excitation", *Eng. Struct.*, **41**, 444-455.
Choi, H. and Kim, J. (2006), "Energy-based seismic design of buckling-restrained braced frames using hysteretic energy spectrum", *Eng. Struct.*, **28**(2), 304-311.
Chou, C.C. and Uang, C.M. (2000), "Establishing absorbed energy spectra-an attenuation approach", *Earthq. Eng. Struct. Dyn.*, **29**(10), 1441-1455.
Decanini, L.D. and Mollaioli, F. (2001), "An energy-based methodology for the seismic assessment of seismic demand", *Soil. Dyn. Earthq. Eng.*, **21**(2), 113-137.
Estes, K.R. and Anderson, J.C. (2002), "Hysteretic energy demands in multistory buildings", *The 7th US national conference on earthquake engineering*, Boston, USA.
Fajfar, P. (1999), "Capacity spectrum method based on inelastic demand spectra", *Earthq. Eng. Struct. Dyn.*, **28**(9), 979-993.
Fajfar, P. and Vidic, T. (1994), "Consistent inelastic design spectra: hysteretic and input energy", *Earthq. Eng. Struct. Dyn.*, **23**(5), 523-537.
Ghosh, S. and Collins, K.R. (2006), "Merging energy-based design criteria and reliability-base methods: exploring a new concept", *Earthq. Eng. Struct. Dyn.*, **35**(13), 1677-1698.
Habibi, A., Chan, R.W.K. and Albermani, F. (2013), "Energy-based design method for seismic retrofitting with passive energy dissipation systems", *Eng. Struct.*, **46**, 77-86.
Hagiwara, Y. (2000), "Momentary energy absorption and effective loading cycles of structures during earthquakes", *The 15th World Conference on Earthquake Engineering*, Auckland, New Zealand.
Kalkan, E. and Kunnath, S.K. (2007), "Assessment of current nonlinear static procedures for seismic evaluation of buildings", *Eng. Struct.*, **29**(3), 305-316.
Kunnanth, S.K. and Chai, H. (2004), "Cumulative damage-based inelastic cyclic demand spectrum", *Earthq. Eng. Struct. Dyn.*, **33**(4), 499-520.
Leelataviwat, S. and Goel, S.C. (2002), "Energy-based seismic design of structures using yield mechanism and target drift", *J. Struct. Eng.*, **128**(8), 1046-1054.
Manoukas, G., Athanatopoulou, A. and Avramidis, L. (2012), "Multimode pushover analysis for asymmetric buildings under biaxial seismic excitation based on a new concept of the equivalent single degree of freedom system", *Soil. Dyn. Earthq. Eng.*, **38**, 88-96.
Poursha, M., Khoshnoudian, F. and Moghadam, A.S. (2011), "A consecutive modal pushover procedure for nonlinear static analysis of one-way unsymmetric-plan tall building structures", *Eng. Struct.*, **33**(9), 2417-2434.
Prasanth, T., Ghosh, S. and Collins, K.R. (2008), "Estimation of hysteretic energy demand using concepts of modal pushover analysis", *Earthq. Eng. Struct. Dyn.*, **37**(6), 975-990.
Riddell, R. and Garcia, J.E. (2001), "Hysteretic energy spectrum and damage control", *Earthq. Eng. Struct. Dyn.*, **30**(12), 1791-1816.
Wang, F. and Li, H.N. (2015), "The method for estimating hysteretic energy of multistory structures based on the normalized hysteretic energy spectra", *J. Vib. Eng.*, **28**(1), 115-121.
Wang, F., Li, H.N. and Yi, T.H. (2015), "Energy spectra of constant ductility factors for orthogonal bidirectional earthquake excitations", *Adv. Struct. Eng.*, **18**(11), 1887-1899.
Wang, F., Sun, J.G. and Zhang, N. (2014), "An improved multidimensional MPA procedure for bidirectional earthquake excitations", *Sci. World J.*, ID 320756.